drones

MDPI

Article

Experimental Investigation on Thrust Performance of a Small-Scale Staggered Rotor System in Hover

He Zhu [1,2], Siqiang Deng [3], Shaoxiong Wei [3], Hong Nie [1,2,*] and Xiaohui Wei [2,4]

[1] National Key Laboratory of Helicopter Aeromechanics, Nanjing University of Aeronautics and Astronautics, Nanjing 210016, China; zhuhe0728@nuaa.edu.cn
[2] Key Laboratory of Fundamental Science for National Defense-Advanced Design Technology of Flight Vehicle, Nanjing University of Aeronautics and Astronautics, Nanjing 210016, China; wei_xiaohui@nuaa.edu.cn
[3] College of Aerospace Engineering, Nanjing University of Aeronautics and Astronautics, Nanjing 210016, China; dengsq@nuaa.edu.cn (S.D.); weishaoxiong@nuaa.edu.cn (S.W.)
[4] State Key Laboratory of Mechanics and Control for Aerospace Structures, Nanjing University of Aeronautics and Astronautics, Nanjing 210016, China
* Correspondence: hnie@nuaa.edu.cn

Abstract: In recent years, the demand for Urban Air Mobility (UAM) and Micro Aerial Vehicles (MAVs) has driven the emergence of new aircraft designs, with the Staggered Rotor System being widely applied in these vertical take-off and landing aircraft. Due to the complex aerodynamic interference between rotors, the spacing between them has a significant impact on the performance of these new aircraft configurations. A testbed was designed and validated to investigate the effects of parameters such as axial distance and lateral distance between rotors on the thrust performance of the Staggered Rotor System. A series of systematic thrust tests was conducted on two co-rotating small-scale rotor models, with particular focus on thrust testing of individual rotors in isolation and their comparison to the conditions of the Staggered Rotor System. During the experimental process, as both the axial and lateral distance varied, an orthogonal experimental design was employed to assess the influence of aerodynamic interactions caused by different rotor diameters on rotor performance. This study conducts an analysis of experimental data to investigate the influence of these factors on the performance of rotor systems' thrust, while also examining the aerodynamic interference and aerodynamic force evolution patterns of rotor systems under varying parameters. Furthermore, rotor speed also plays a crucial role in the performance of the system. Therefore, when designing vertical take-off and landing aircraft with multiple rotors, it is essential to consider the influence of these factors during the optimization process.

Keywords: aerodynamics; propulsion system; MAV; staggered rotor

check for updates

Citation: Zhu, H.; Deng, S.; Wei, S.; Nie, H.; Wei, X. Experimental Investigation on Thrust Performance of a Small-Scale Staggered Rotor System in Hover. *Drones* **2023**, *7*, 677. https://doi.org/10.3390/drones7110677

Academic Editor: Mostafa Hassanalian

Received: 13 October 2023
Revised: 10 November 2023
Accepted: 14 November 2023
Published: 15 November 2023

1. Introduction

There has been an abundance of new and novel aircraft designs [1–4] created for UAM in recent years. Several conceptual designs or prototypes have been unveiled by manufacturers such as Rolls-Royce [5], Uber [6], Airbus and Volocopter GmbH. Volocopter GmbH has introduced a very promising concept, the VC2X, featuring 18 rotors [7]. Aircraft that are utilized for UAM require outstanding aerodynamic performance which is closely related to their propulsion system [8,9]. Due to restrictions on take-off and landing sites, UAM aircraft require a vertical take-off and landing ability as well [10], which widely relies on multi-rotor power systems in various configurations.

Compared to traditional helicopters with a single rotor and tail rotor system configuration, which are limited by blade tip velocity, electric Vertical Take-off and Landing vehicles (eVTOLs) equipped with multiple rotor systems could operate at higher speeds [10,11]. However, there are certain challenges involved in the studies of eVTOLs. Unlike in fixed-wing vehicles or even rotary-wing vehicles in forward flight, the flowfield of hovering rotors is significantly influenced by the trailed wake system since it remains in the proximity of the rotor at all times [12,13]. Additionally, the effect of the wake is highly significant since one is interested in its interaction with the rotor blades. Therefore, an accurate representation of the rotor system thrust formation and evolution is essential in achieving high-fidelity performance predictions of hovering MAVs.

A coaxial rotor configuration, the interaction between the two rotors and their wakes [14,15], creates a more complex airflow pattern compared to a single-rotor system. A substantial part of the bottom rotor consistently operates within the top rotor's wake. This significantly impacts the distribution of incoming air across the entire system [16] and affects the boundary layer of the bottom rotor blades. Generally, this interaction can lead to a reduction in the overall aerodynamic efficiency of the rotor system and, even during hovering, can cause undesirable fluctuations in the airflow. Aerodynamics and flow physics of either microscale single rotors or full-scale coaxial rotors are relatively less studied and understood. With the growing desire for efficient rotary-wing MAVs, which typically operate at Re 10^3–10^5, accurate predictions of low-Mach, viscous-dominated flows are in increasing demand. Because of the difficulties involved in computationally studying MAVs for this Reynolds number range, accurate experimental results are of critical importance to eVTOL research. Furthermore, accurate numerical schemes and reliable turbulence models need to be used and the resulting methodology needs to be carefully validated with experiments if the Computational Fluid Dynamics (CFD) results are to be considered reliable [17].

Many scholars [15,18–20] have analyzed aerodynamic performance in different flight conditions for coaxial configurations using the CFD method. Zhang [21], Grace [22] and Tugnoli [23] et al. employed various CFD tools to simulate rotorcraft flow and analyzed the influence of the rotor–airframe interaction. In the study of unsteady performance, the use of CFD methods is essential. However, in attempting to establish precise numerical models, reliable experimental data validation is crucial. Although numerical analysis methods such as CFD have advanced rapidly [24–26], accurately modeling the aerodynamic performance of rigid coaxial rotors remains a significant challenge. Experimental testing continues to be an indispensable approach for studying the aerodynamics of these rotors. Bohorquez et al. employed a computerized hover test stand for systematic testing of both single and coaxial small-scale rotors. Their research delved into the impact of airfoil geometry, blade manufacturing techniques and rotor configurations [27]. Ramasamy carried out a series of experiments to assess the performance of various rotor configurations, encompassing single, coaxial, tandem and tilt rotors, employing both untwisted and highly twisted blades [28]. Recently, to investigate the aerodynamic interaction between tandem overlapping propellers in eVTOL-airplane-mode flight conditions, Zanotti and their team conducted a series of systematic wind tunnel experiments to validate the impact on propeller performance and the flow field [29].

Staggered rotor systems, which involve multiple rotor blades that are not aligned in the same plane, can have various implications on aircraft performance and control. In the authors' previous research, significant impact of the staggered rotor power system was identified on the aircraft's overall aerodynamic performance [30], optimization design [31,32], controller design and flight quality [33]. In order to help find superior performance in multi-rotor configurations, many scholars have conducted research related to overlapping rotors to enhance and optimize aircraft design. Otsuka [34] evaluated the effect of rotor flow interactions on thrust for three two-rotor configurations. Buzzatto [35] designed an open-source benchmarking platform to analyze and improve the efficiency of coaxial rotor systems. Weishupl [36] investigated the interference that arises from overlapping UAV propellers during hovering flight and found that the overlapping region (0–20%) can increase hover flight endurance. Mantas [37] et al. analyzed the impact of vertical spacing on the overlapping thrust sharing between upper and lower rotors in a coaxial system using a systematic torque balance model.

This paper introduces a thrust testbed designed for staggered rotor tension systems and conducts relevant experimental research. The goal of this work is to study the performance and flow physics of a microscale staggered rotor system, with a particular focus on the effects of lateral and axial distance on the system. This will help in determining the feasibility and performance of using a staggered rotor configuration for eVTOLs and MAVs. The experiments are outlined first, encompassing the analysis of the flow model, the composition and operational principles of the test rig, as well as the selection and design of experimental parameters. Subsequently, the precision of the experimental setup is validated, and an analysis of experimental errors is conducted. Next, a detailed discussion is provided regarding the influence patterns of three parameters: rotational speed, lateral distance and axial distance. A comparative analysis is conducted between single-rotor and dual-rotor systems. Finally, conclusions derived from the aforementioned research and analysis are presented.

2. Experiments

2.1. Experiment Setup

The flow models for coaxial rotor systems and staggered rotor systems are shown in Figure 1; the wake from the top rotor is found to contract quickly, while the bottom rotor operates partially within the developed wake of the top rotor [38]. The staggered rotor system, due to the interweaving distribution of rotors, results in a more complex flow.

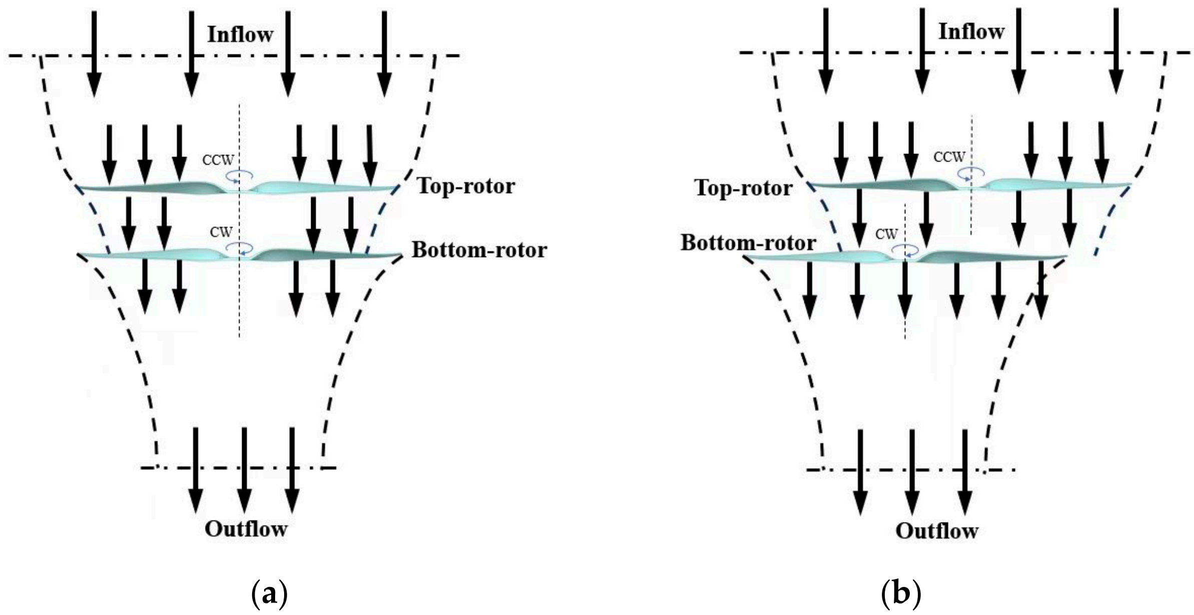

Figure 1. Flow models of coaxial rotor systems and staggered rotor systems. (**a**) Coaxial rotor system; (**b**) staggered rotor system.

The experiment utilized commercially available T-MOTOR 1855 carbon fiber integrated propellers known for their high strength and low weight. These propellers consist of two blades with a diameter of 18 inches (457.2 mm) and a pitch (also referred to as propeller pitch) of 5.5 inches (139.7 mm). The weight of a single propeller blade is approximately 37 g. To facilitate the description of the relationship between spacing and rotor radius, we define 'h' as h = H/R, where H represents the axial distance between the top and bottom rotors and R is the rotor's radius. Similarly, 'l' is defined as l = L/R, with L denoting the lateral distance between the centers of the top and bottom rotors and R being the rotor's radius, as in Figure 2.

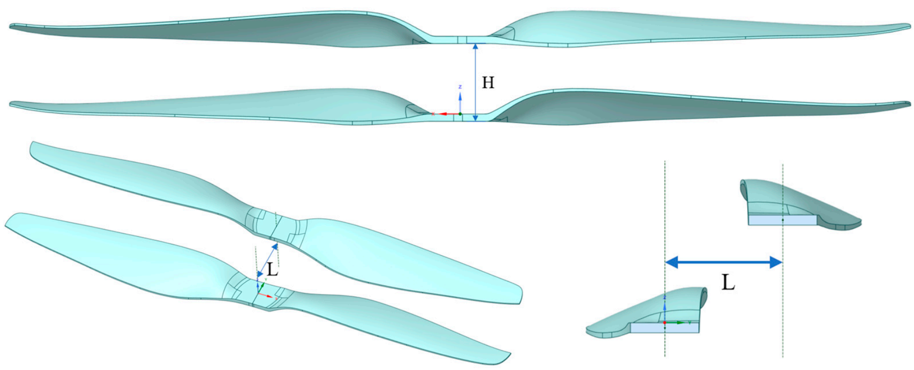

Figure 2. Representation of rotor axial distance and lateral distance.

The experiment was conducted by varying the rotational speed (Revolutions Per Minute, RPM) from approximately 500 RPM to 3500 RPM. Consequently, the blade tip Reynolds number ranged from 0.16 × 105 to 1.15 × 105, the blade tip Mach number varied from 0.04 to 0.25, and the blade tip velocity ranged from 12 m/s to 84 m/s. Note that, when viewed from above, the top rotor rotates in an counterclockwise fashion and the bottom rotor rotates clockwise. Figure 3b is an overview of the testbed, while Figure 3c,d shows close-up views. By adjusting the bolts in Figure 3c to change the platform's position, the axial distance h between the rotors is altered; and by adjusting the slider position in Figure 3d, the lateral distance l between the rotors is modified.

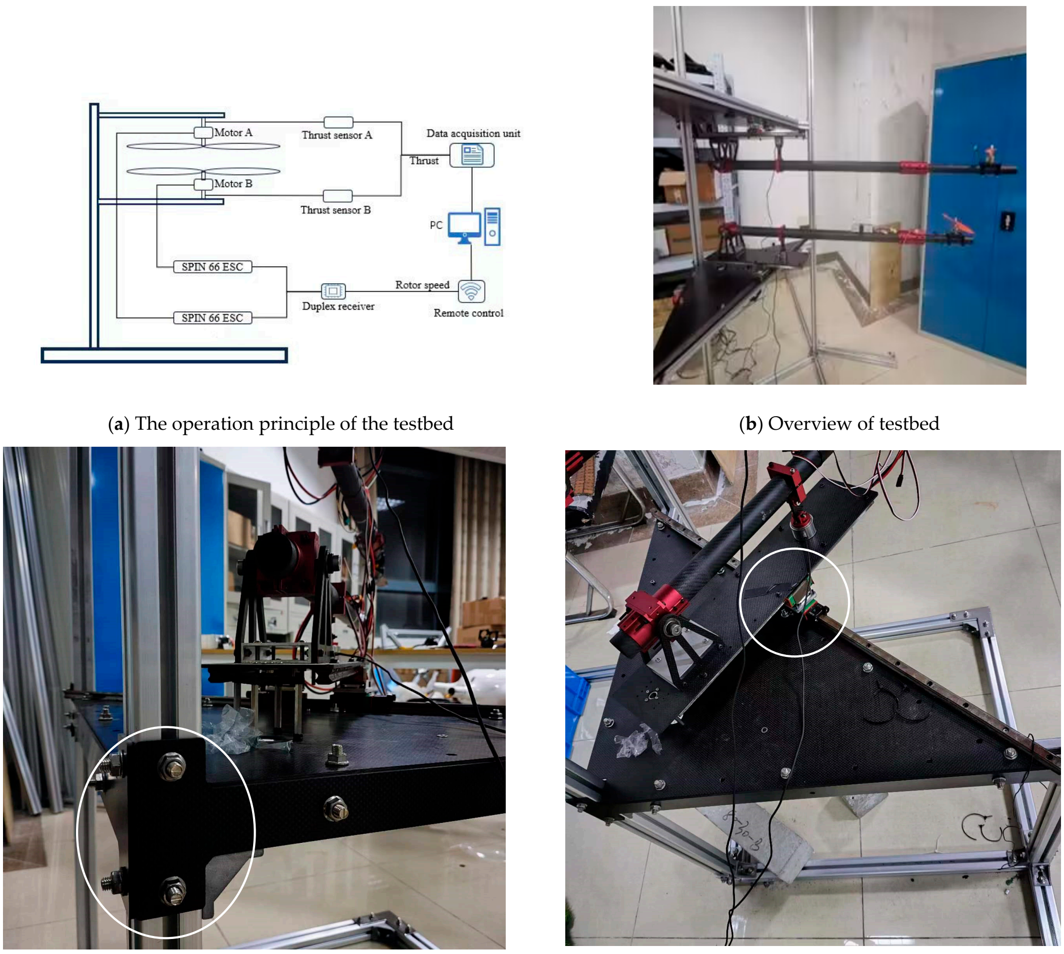

(**a**) The operation principle of the testbed

(**b**) Overview of testbed

(**c**) Adjustment of h

(**d**) Adjustment of l

Figure 3. Experimental setup.

The operation principle of the experimental setup is depicted in Figure 3a. The top and bottom dual rotors are connected to motors and tension sensors, securely mounted on the testbed to measure the thrust generated during their rotation. In order to mitigate the potential interference of the natural frequencies of the experimental setup with measurement results, the authors conducted vibration tests using specialized equipment under ambient room temperature conditions. The measured second-order natural frequencies of the test rig were determined to be 93 Hz and 154 Hz, while the maximum rotor frequency under all experimental conditions was 58.3 Hz. Consequently, it can be concluded that the natural frequencies of the experimental setup, as illustrated in Figure 3, are not prone to causing interference with measurements under any operating conditions. During the experiment, when the throttle lever on the remote controller is pushed, the receiver receives the signal and controls the motor's rotation through an Electronic Speed Controller (ESC), simultaneously displaying real-time rotor speed. At the same time, a tension sensor measures the rotor's thrust and transmits these data to a computer via a data collector, recording both the speed and thrust values. The main components of the experimental setup include: TATTU 22.8 V 6S1P 25000 mAh 10C High Voltage Lipo Battery (Geshi ace, Shenzhen, China); T-MOTOR 1855 propellers (T-motor, Nanchang, China); JFRC U4114 brushless DC motor (KV: 320 RPM/V) (RCmodel, Yongzhou, Chnia); ZNLBM-IIX tension sensor (sensitivity: 1.5 mV/V) (Shenghongchuang, Xi'an, China); Master SPIN 66 Pro ESC (capable of real-time feedback on speed, battery voltage, temperature, etc.) (JETI model, Hong Kong, China); JETI BOX programming controller; JETI DUPLEX channel receiver (signal processing and switching) (JETI model, Hong Kong, China); and JETI DUPLEX 2.4 EX remote controller (signal input and status monitoring) (JETI model, Hong Kong, China).

2.2. Design of Experiment

The range of parameter values explored in the experiment is presented in Table 1. Due to the potential geometric interference between the two rotors caused by variations in blade thickness, the axial distance between the two rotors was initially set at 0.3. The values for lateral distance form an arithmetic sequence between 0 and 2.4, with a common difference of 0.4 between adjacent values. In previous flight research experiments on staggered rotor unmanned aerial vehicles [31,33], corresponding reference values for rotor speed under no load operation were identified. As such, the primary testing range for rotor speed falls between the commonly encountered values of 2000 and 3500 RPM in the operational state of this type of rotor. Within this parameter range, the aerodynamic thrust on the rotor is relatively higher, and its characteristics become more pronounced.

Table 1. Design of experiments.

Variables	Values
h	0.3, 0.4, 0.5, 0.6, 0.8
l	0, 0.4, 0.6, 1.2, 1.6, 2.0, 2.4
RPM	2000, 2500, 3000, 3500

3. Error Analysis and Verification

In order to enhance the accuracy and reliability of the experimental results, error analysis was conducted on the testbed. The industrial-grade ZNLBM-IIX tension sensor (Shenghongchuang, Xi'an, China) used in the experiment has an error rate of less than 1%, indicating a high level of accuracy. To ensure the precision of the measurement data, a 1 kg calibration weight was directly applied to verify its accuracy. The average of multiple measurements with the calibration weight was found to be 1.002 kg, with an error of less than 0.5%. This suggests that the sensor's measurement accuracy meets the experimental requirements.

In addition to the tension sensor error, there is also an error associated with the measurement of rotor speed. The error in the rotor speed measurement is related to the number of magnets in the rotor. The motor's slot–pole structure is 12N14P, meaning it has 14 magnets in total. Therefore, the accuracy at any given rotor speed is 1/14. This results in a speed measurement error of approximately 4.26 RPM (1/14 × 60 RPM) at any given speed.

In addition, the thrust coefficient (y) is derived through indirect calculations based on the direct measurements of thrust (x_1) and the corresponding rotor speed (x_2). According to the uncertainty calculation method proposed by Kline and McClintock [39] (1953), when a variable y is obtained indirectly from n direct variables x_i, its uncertainty can be determined using the following formula:

$$u_y^2 = \left(\frac{\partial y}{\partial x_1} u_{x_1}\right)^2 + \left(\frac{\partial y}{\partial x_2} u_{x_2}\right)^2 + \cdots + \left(\frac{\partial y}{\partial x_n} u_{x_n}\right)^2 \tag{1}$$

When we substitute the thrust coefficient, we obtain:

$$\Delta C_T^2 = \left(\frac{1}{\rho A (\Omega R)^2} \Delta T\right)^2 + \left(\frac{-2}{\rho A \Omega^3 R^2} \Delta\Omega\right)^2 = \left(\frac{C_T}{T} \Delta T\right)^2 + \left(\frac{-2C_T}{\Omega} \Delta\Omega\right)^2 \tag{2}$$

$$\frac{\Delta C_T}{C_T} = \sqrt{\left(\frac{\Delta T}{T}\right)^2 + 4\left(\frac{\Delta\Omega}{\Omega}\right)^2} \tag{3}$$

When we substitute the measured thrust and rotor speed from the experiments, we calculate that the maximum error for the thrust coefficient in this study is 1.2%.

4. Results and Analysis

Before measuring the coaxial dual-rotor thrust, it is essential to separately measure the thrust of each rotor operating at different speeds. This serves two purposes: first, it allows us to validate whether the measured data align with theoretical formulas, and second, it helps optimize the system structure to eliminate the aerodynamic interference between the rotor and the testbed. The measured thrust for the top and bottom rotors is depicted in Figure 4, and the formula for rotor thrust [40] is as follows:

$$T = \frac{1}{2} \rho \pi R^2 (\Omega R)^2 C_T \tag{4}$$

Here, ρ represents density, R is the rotor radius, Ω is the rotor angular velocity and C_T is the thrust coefficient. From the formula, it is evident that rotor thrust is directly proportional to the square of the rotor speed. Figure 4 presents the variation of thrust for an isolated single upper (lower) rotor as a function of rotor speed. It is important to note that the individual thrust of the upper and lower rotors was measured in the absence of another rotor. The experimental curve closely approximates a quadratic curve, aligning with the rotor thrust formula.

From Figure 4, it is observable that the thrust produced when the top and bottom rotors operate individually is nearly identical, with the bottom rotor thrust slightly lower than the top rotor. This difference is attributed to the rotor support structure of the testbed, which affects the inflow for the top rotor and outflow for the bottom rotor, resulting in a slight influence on rotor thrust. However, the thrust measurements for both top and bottom rotors exhibit an error of less than 2%. Therefore, we can conclude that the rotor thrust data obtained from the testbed are reliable and accurate.

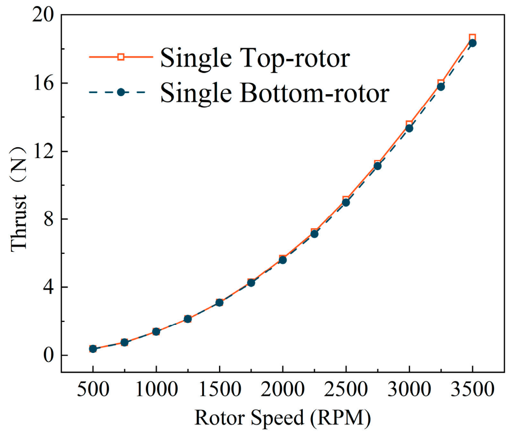

Figure 4. Single-rotor thrust variation.

Figure 5 illustrates the thrust coefficient for individual top and bottom rotors at different speeds. The formula used to calculate the thrust coefficient is as follows:

$$C_T = \frac{T}{\rho A(\Omega R)^2} = \frac{T}{\rho \pi \Omega^2 R^4} \tag{5}$$

From Figure 5, it is evident that the thrust coefficient for the bottom rotor is slightly lower than that of the top rotor across the entire range of rotor speeds, consistent with the earlier thrust analysis results.

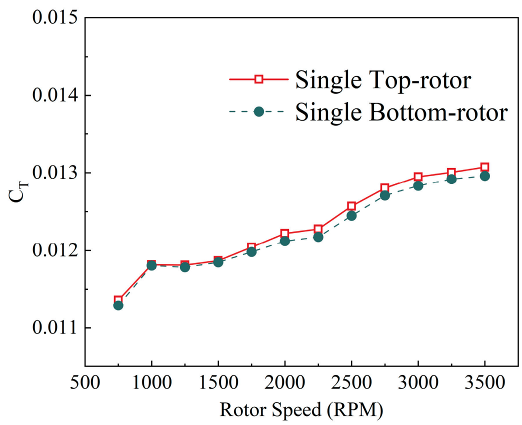

Figure 5. Single-rotor C_T variation.

Reynolds number is a dimensionless number used to characterize fluid flow, indicating the ratio of inertial forces to viscous forces acting on an object. Its calculation formula is as follows:

$$Re = \frac{\rho V l}{\mu} \tag{6}$$

Here, ρ represents the density of the fluid (air), V denotes the magnitude of flow velocity, l stands for the characteristic length of the object and μ represents the fluid viscosity. It can be observed that the thrust coefficient exhibits a slight linear increase with rotor speed. This is attributed to the relatively low Reynolds number conditions in this experiment. At low Reynolds numbers, viscous effects dominate the flow, making it prone to airflow separation, thereby reducing rotor efficiency. As rotor speed increases, the inertial effects of the fluid become relatively stronger while viscous effects weaken. Consequently, the rotor's performance improves, resulting in a slight increase in the thrust coefficient. This is a characteristic feature of rotors operating at low Reynolds numbers [28].

Thrust is the most direct factor determining the load on a rotor system. Over the course of a rotor's rotation cycle, there are periodic thrust fluctuations due to the effects of load and thickness [41]. Specifically, when the top and bottom blades are very close together, the thickness of the blades affects the thrust. This results in negative impulse-like fluctuations in the thrust of the top rotor and positive impulse-like fluctuations in the thrust of the bottom rotor. Additionally, rotor thrust is influenced by the load effects generated by blade attachment vorticity. When the top and bottom rotors approach each other, they induce an upwash flow in each other's vicinity. The upwash flow initially increases and then decreases, eventually turning into a downwash flow at a certain point. The strength of the downwash flow first increases and then decreases as the rotors move away from each other. Consequently, when the blades come close to each other and then move apart, the thrust on both the top and bottom rotors initially increases, then decreases, and then increases again, exhibiting periodic fluctuations. In the experiment, it can be challenging to accurately capture the periodic fluctuation curves. Therefore, taking the median value of the thrust is a practical approach.

4.1. Effects of Rotor RPM

The rotor speed is a critical parameter for the performance and operation of rotorcraft. Operators and engineers need to select the appropriate speed based on specific tasks and flight conditions to achieve optimal flight performance and efficiency. Figure 6 illustrates the measured results of coaxial dual-rotor thrust as a function of rotor speed. Both top and bottom rotors exhibit approximately quadratic trends. However, there are differences between them. The top rotor maintains relatively consistent thrust levels and trends at various lateral distances, with minor variations at high speeds.

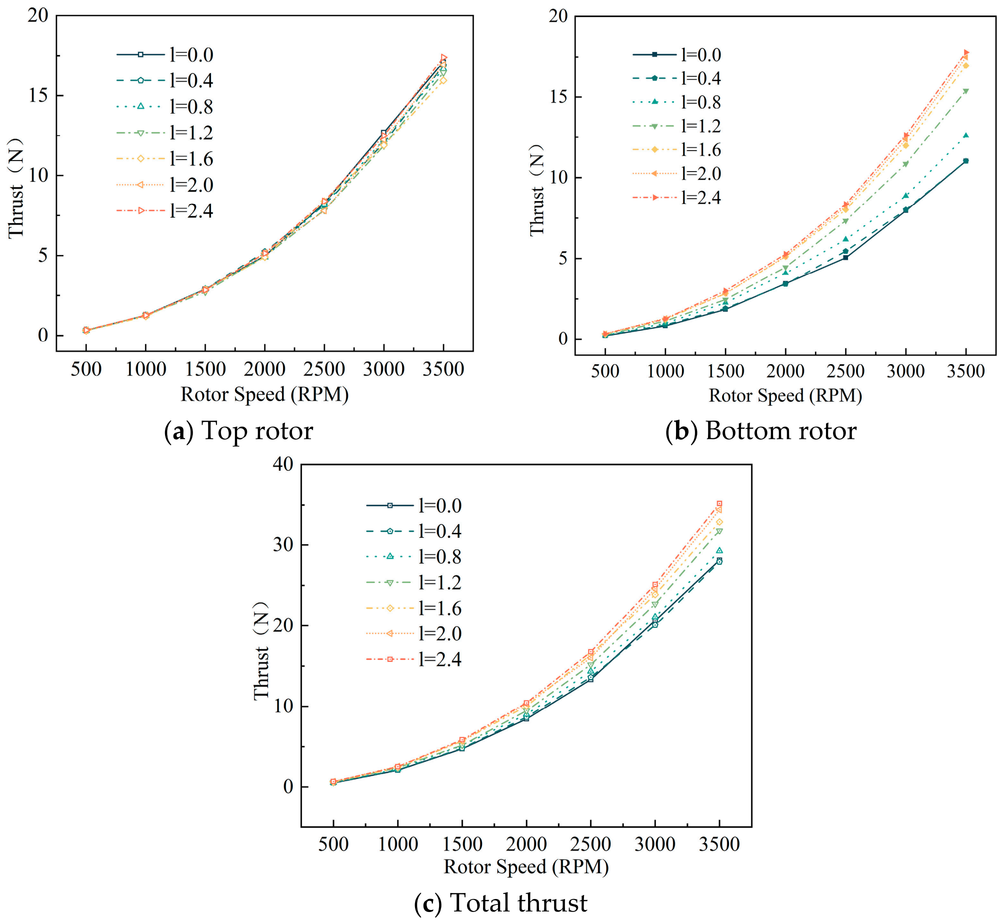

Figure 6. The variation of thrust with rotor speed at an axial distance (h) of 0.3.

In contrast, the bottom rotor experiences significant changes in thrust as lateral distance varies. As the lateral distance increases, the thrust of the bottom rotor increases at the same rotor speed. When the lateral distance reaches 1.6 times the rotor radius or higher, the thrust trends become almost identical. This is primarily due to the reduced impact of the downward airflow generated by the top rotor on the inflow of the bottom rotor, as depicted in Figure 1b. When the lateral distance (l) exceeds 1.6, the influence of the top rotor on the bottom rotor is nearly negligible, resulting in consistent thrust trends for the bottom rotor, as shown in Figure 7. During this phase, the top and bottom rotor curves essentially overlap, although they both remain slightly lower than that of a single rotor, indicating residual aerodynamic interference leading to reduced thrust. While the thrust of the top rotor remains relatively stable with changes in lateral distance, with variations within 4% of the mean thrust at high speeds, the thrust of the bottom rotor exhibits more significant variations.

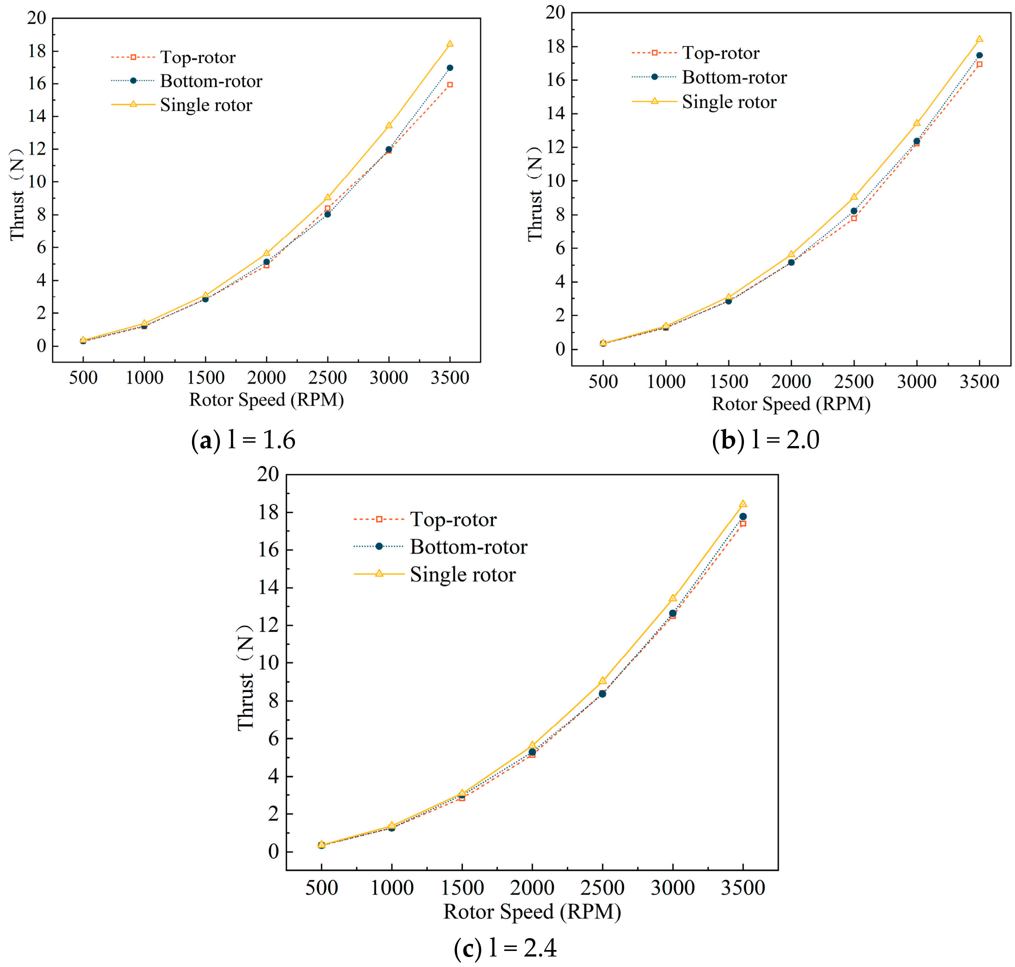

Figure 7. The variation of thrust with rotor speed at different lateral distances.

Figure 8 illustrates the thrust coefficient for both top and bottom rotors when operating simultaneously at different rotor speeds. It is evident that the thrust coefficient for the top rotor remains within a consistent range across various lateral distances, following a trend that aligns with the behavior observed when the rotor operates independently. In contrast, the bottom rotor experiences an increase in thrust coefficient with increasing lateral distance. At the same lateral distance, the trend in thrust coefficient change with respect to rotor speed for the bottom rotor also mirrors that of a single rotor.

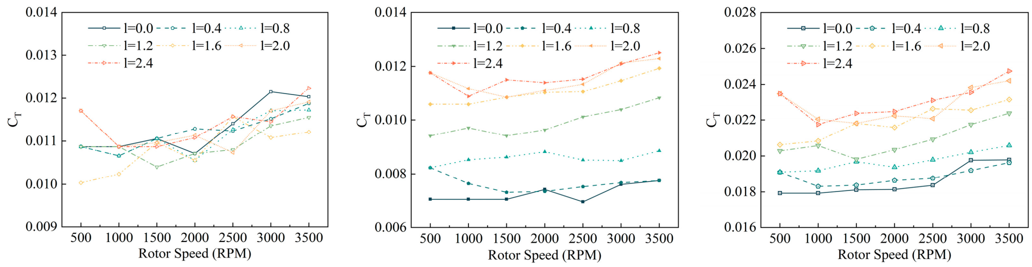

(**a**) l = 1.6 (**b**) l = 2.0 (**c**) l = 2.4

Figure 8. The rotor thrust coefficient variation with rotor speed at different lateral distances with an axial distance (h) of 0.3.

To better investigate the aerodynamic interference effects between the upper and lower rotors concerning rotor speed, experiments were conducted with the lower rotor speed fixed at 2000 RPM. In one set, the upper rotor speed varied from 1500 RPM to 3500 RPM, and the measurement results are illustrated in Figure 9a. In another set, the lower rotor speed varied from 1500 RPM to 3500 RPM, with the upper rotor speed fixed at 2000 RPM, and the corresponding measurement results are depicted in Figure 9b.

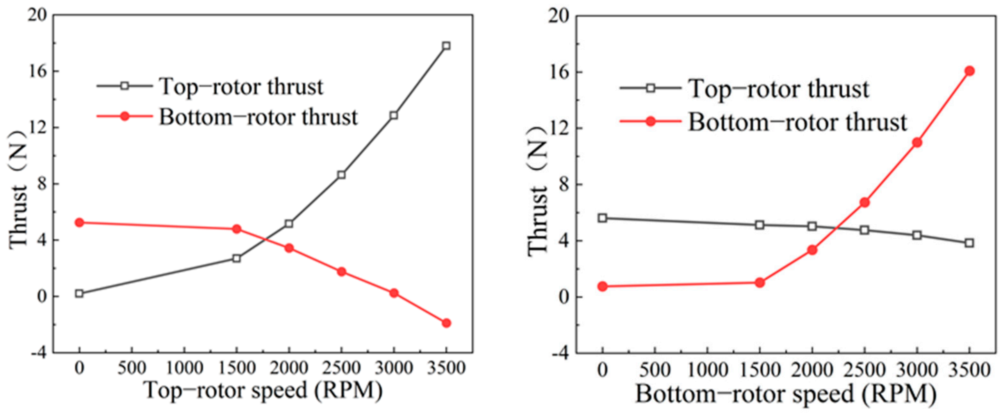

(**a**) l = 1.6 (**b**) l = 2.0

Figure 9. The variation of rotor thrust with rotational speed at a fixed speed for a single rotor.

When the upper rotor is stationary (0 RPM) while the lower rotor is rotating at 2000 RPM, the inflow generated by the rotating lower rotor results in a slight downward thrust on the upper rotor, approximately 0.2 N. Conversely, when the lower rotor is stationary (0 RPM) while the upper rotor is rotating at 2000 RPM, the outflow generated by the rotating upper rotor imparts a downward thrust on the lower rotor, measuring 0.75 N. This observation indicates that, under the same conditions, the outflow has a greater impact than the inflow on rotor interactions. This insight also reflects the greater influence of the upper rotor on the lower rotor in a coaxial configuration.

Furthermore, comparing Figure 9a,b reveals that increasing rotor speed leads to a reduction in thrust on the fixed-speed rotor. The upper rotor's variation in speed has a more pronounced effect on the lower rotor, resulting in a decrease in thrust of 7.15 N compared to the 0 RPM condition. In contrast, the lower rotor's variation in speed has a relatively smaller impact on the upper rotor, causing a decrease in thrust of only 1.77 N compared to the 0 RPM condition.

4.2. Effects of Axial Distance

In the research of coaxial rotorcraft, the axial distance between the top and bottom rotors plays a significant role in flight performance, maneuverability and stability. Typically, continuous adjustments of the rotor spacing are necessary to optimize the design and performance of the aircraft. Therefore, it is essential to investigate the impact of axial distance to provide insights for the design of coaxial rotorcraft. To characterize the influence of axial distance on rotor thrust at different speeds, we define a thrust variation coefficient ΔT:

$$\Delta T = (Tmax - Tmin)/Tave \tag{7}$$

For the same rotor speed and axial distance parameters, $Tmax$ represents the maximum thrust of the bottom rotor at different lateral distances, $Tmin$ represents the minimum thrust of the rotor at various lateral distances, and $Tave$ is the average thrust of all rotor systems. After data processing, the results are presented in Table 2.

Table 2. ΔT of bottom rotor in coaxial system.

h	2000 RPM (ΔT)	2500 RPM (ΔT)	3000 RPM (ΔT)	3500 RPM (ΔT)	$\Delta Tave$
0.3	0.430	0.451	0.492	0.467	0.46
0.4	0.578	0.527	0.550	0.606	0.56525
0.5	0.546	0.534	0.548	0.497	0.53125
0.6	0.610	0.578	0.576	0.607	0.59275
0.8	0.582	0.566	0.677	0.661	0.6215
ΔT_{ave}	0.5492	0.5312	0.5686	0.5676	

When observing the evolution of ΔT (the change in thrust) for the bottom rotor in the coaxial system, it becomes evident that it does not exhibit a strictly linear trend, as depicted in Figure 10. When the axial distance shifts from 0.3 to 0.4, ΔT increases for various rotor speeds. However, when the axial distance becomes 0.5, there is no clear pattern in the change of ΔT across different speeds. Nevertheless, looking at the overall trend, the magnitude of thrust variation remains relatively stable with changes in rotor speed but generally increases with variations in axial distance. This suggests that when the axial distance is larger, the bottom rotor experiences greater thrust variations across different lateral distances.

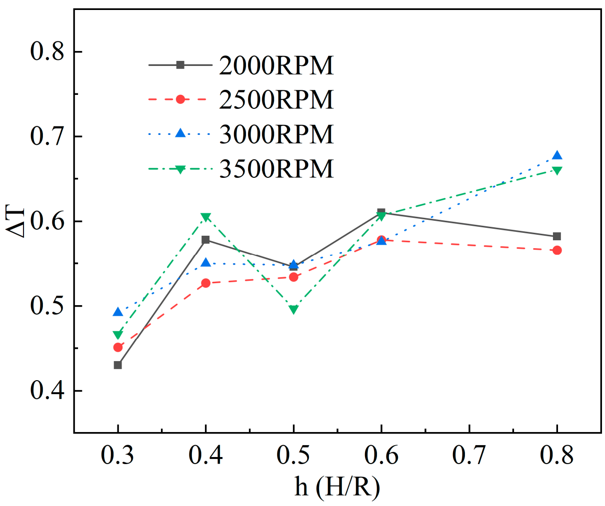

Figure 10. The variation of ΔT with axial distance at different speeds.

In the case of coaxial configurations, aerodynamic interference alters the distribution of thrust between the top and bottom rotors. This distribution varies with changes in axial distance. To investigate how thrust distribution changes with axial distance (h = 0.2, 0.3, 0.35, 0.4, 0.5 and 0.6), we conducted experiments at a controlled rotor speed of 2000 RPM, resulting in tip Reynolds numbers of 0.98×10^5 and tip Mach numbers of 0.14, as shown in Table 3. At smaller axial distances, the top rotor contributes approximately 57% to the total thrust, but as the axial distance increases, the contribution of the top rotor to total thrust also increases, reaching around 64%. As axial distance increases, the measured thrust for the top and bottom rotors exhibits opposite trends. The thrust of the top rotor increases with axial distance, while the thrust of the bottom rotor decreases. Due to the opposing trends in top and bottom rotor thrust, the total thrust of the entire system remains relatively stable with increasing rotor axial distance. This finding aligns with the conclusions drawn by Lakshminarayan in their simulation analysis of coaxial small-scale rotors [41]. The reason behind this phenomenon lies in the aerodynamic interference between the top and bottom rotors. The wake of the top rotor contracts faster compared with that of the bottom rotor because of the vortex–vortex interaction. Further, the top rotor wake convects vertically down at a faster rate due to increased inflow [41]. Due to the rotational motion of the top rotor, it accelerates the airflow beneath it, affecting the inflow to the bottom rotor and leading to reduced aerodynamic efficiency. As the axial distance increases, the outflow from the top rotor improves, moving more swiftly towards the bottom rotor, further decreasing the thrust coefficient of the bottom rotor. When the axial distance reaches a certain level, the outflow velocity of the top rotor no longer increases. At this point, the thrust coefficient of the bottom rotor stabilizes.

Table 3. The rotor thrust at different axial distances (R = 9 in).

h (H/R)	Top Rotor Thrust (N)	Bottom Rotor Thrust (N)	Total Thrust (N)	Top/Total
0.2	4.95	3.72	8.67	57%
0.3	4.97	3.58	8.56	58%
0.35	5.19	3.17	8.36	62%
0.4	5.43	3.07	8.51	64%
0.5	5.31	3.11	8.42	63%
0.6	5.48	3.11	8.59	64%

Figure 11 illustrates the distribution of thrust coefficients with varying axial distances at the same lateral distance for different rotor speeds. In the coaxial configuration, thrust coefficients for both top and bottom rotors increase with higher rotor speeds, consistent with the previously observed trend of thrust coefficient increasing with rotor speed for single rotors. Additionally, it is noteworthy that the thrust coefficient for the top rotor gradually increases with axial distance, while for the bottom rotor, it decreases with increasing axial distance. At a lateral distance of 0.8, the thrust coefficient for the top rotor resembles that of the coaxial configuration, whereas for the bottom rotor, it overall increases. Nevertheless, the trend remains a decrease in thrust coefficient with higher axial distance. This change is due to the reduced impact area of the top rotor outflow on the bottom rotor as the lateral distance increases, somewhat improving its performance and resulting in an overall increase in thrust coefficient.

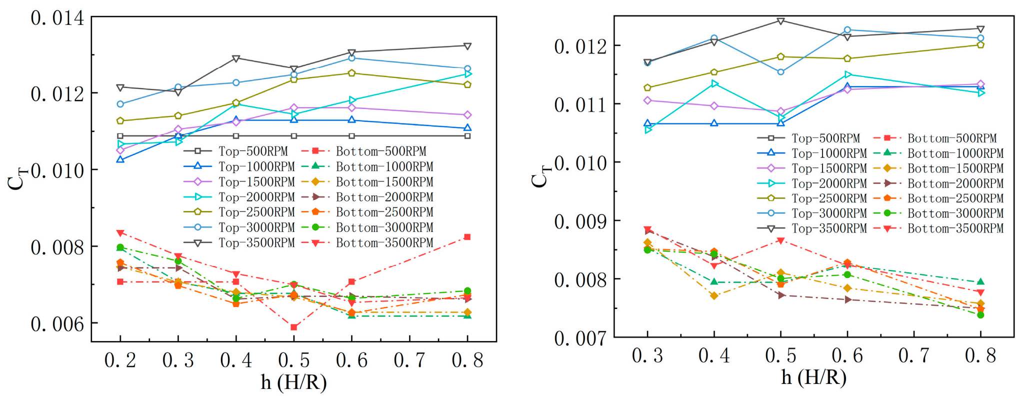

(**a**) l = 0 (**b**) l = 0.8

Figure 11. The variation of thrust coefficient with axial distance for lateral distances of 0 and 0.8.

In the case of a relatively small lateral range, the thrust of the bottom rotor tends to be significantly lower than that of the top rotor. This disparity can be attributed to the varying degrees of influence from the downwash airflow generated by the top rotor. As the lateral distance between rotors increases, the thrust of the bottom rotor gradually rises, and this trend remains consistent across different rotor speeds. The top rotor experiences different variations under the influence of the inflow from the bottom rotor at various speeds, but the magnitude of variations remains within 10% of the top rotor's thrust. The total thrust increases as the spacing between rotors widens, and this trend is further enhanced with increasing rotor speed.

At a fixed rotor speed of 2500 RPM for both rotors, the thrust coefficient variation with axial distance is depicted in the Figure 12 for different lateral distances. The thrust coefficient for the top rotor exhibits relatively minor changes with varying lateral distances, whereas the thrust coefficient for the bottom rotor increases as the lateral distance becomes larger. When the lateral distance is less than 1.6, the overall trend for the top rotor's thrust coefficient increases with increasing axial distance, while the bottom rotor's thrust coefficient decreases with axial distance. However, when the lateral distance is greater than 1.6, the influence of axial distance becomes less pronounced. Across the entire range of axial distances, the thrust coefficients for both top and bottom rotors are lower than those of a single rotor operating independently.

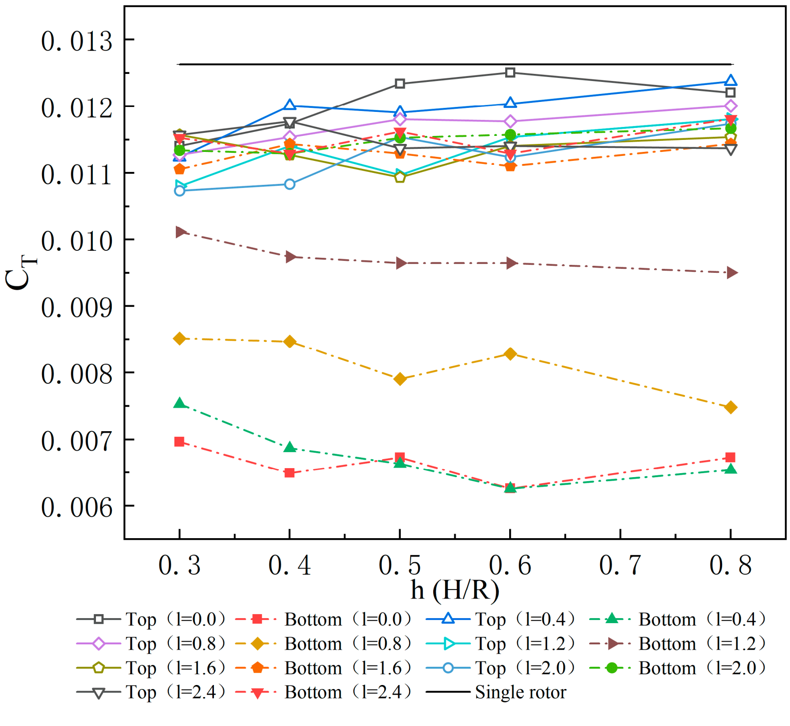

Figure 12. The variation of thrust coefficient with axial distance at a rotor speed of 2500.

4.3. Effects of Lateral Distance

Figure 13 depicts the variation in thrust with increasing lateral distance when the axial distance is set at 0.3 (h = 0.3). As the lateral distance increases, the interference between rotor wakes diminishes. Consequently, the difference in thrust between the top and bottom rotors decreases with the widening lateral distance and nearly disappears at a lateral distance of 1.6. It is worth noting that due to the mutual induction of rotor tip vortices, the thrusts of the top and bottom rotors approach each other at a lateral distance of 1.6. At 2.0, the bottom rotor's thrust surpasses that of the top rotor, and at 2.4, they converge once more.

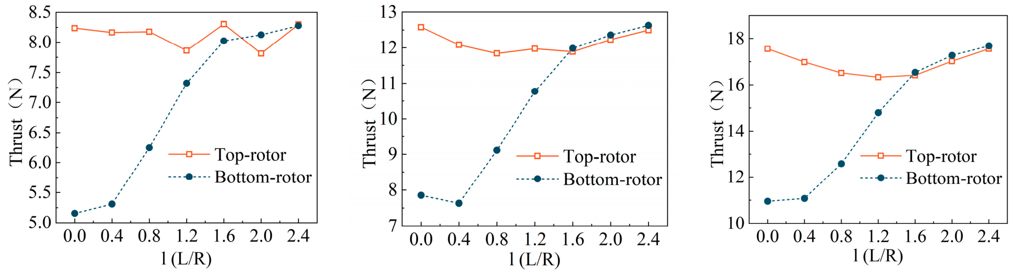

(**a**) RPM = 2500 (**b**) RPM = 3000 (**c**) RPM = 3500

Figure 13. Rotor thrust variation with lateral distance.

Due to the aerodynamic viscosity effects of rotor blades at low Reynolds numbers, the thrust for both top and bottom rotors increases with the widening lateral distance at low rotor speeds. Consequently, the total thrust also increases overall with increasing lateral distance, and this phenomenon becomes more pronounced at higher rotor speeds, as depicted in Figure 14.

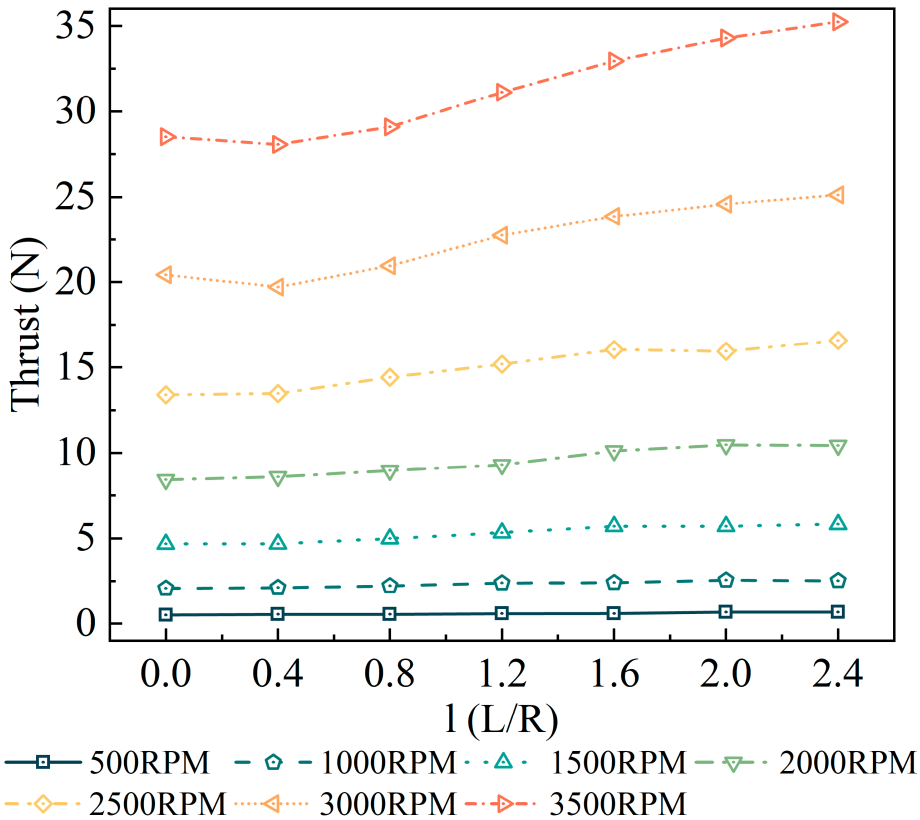

Figure 14. The total rotor thrust variation with lateral distance.

We define the rate of change of thrust with respect to lateral distance as follows:

$$T' = \frac{T - T_{min}}{T_{max} - T_{min}} \tag{8}$$

From Figure 15, it is evident that when the rotor speed surpasses 3000 RPM, there is a downward trend in thrust at a lateral distance of 0.4. However, in all other conditions, rotor thrust increases with the widening of the lateral distance.

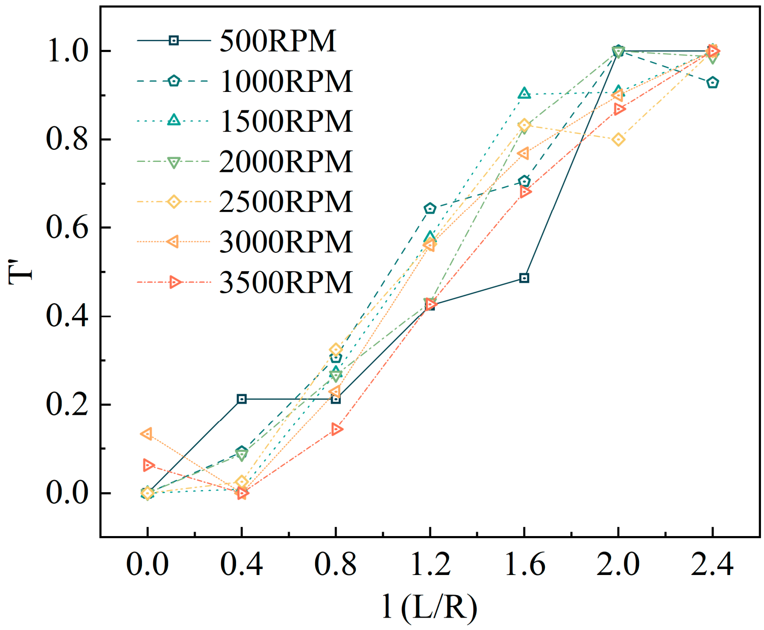

Figure 15. T′ at different lateral distances.

Within the selected parameter range, the change in rotor system thrust remains relatively modest as the axial distance varies. This phenomenon is consistent across different lateral distance conditions, as illustrated in Figure 16. Specifically, the thrust of the top rotor fluctuates within a narrow range, typically within 5% of the average thrust.

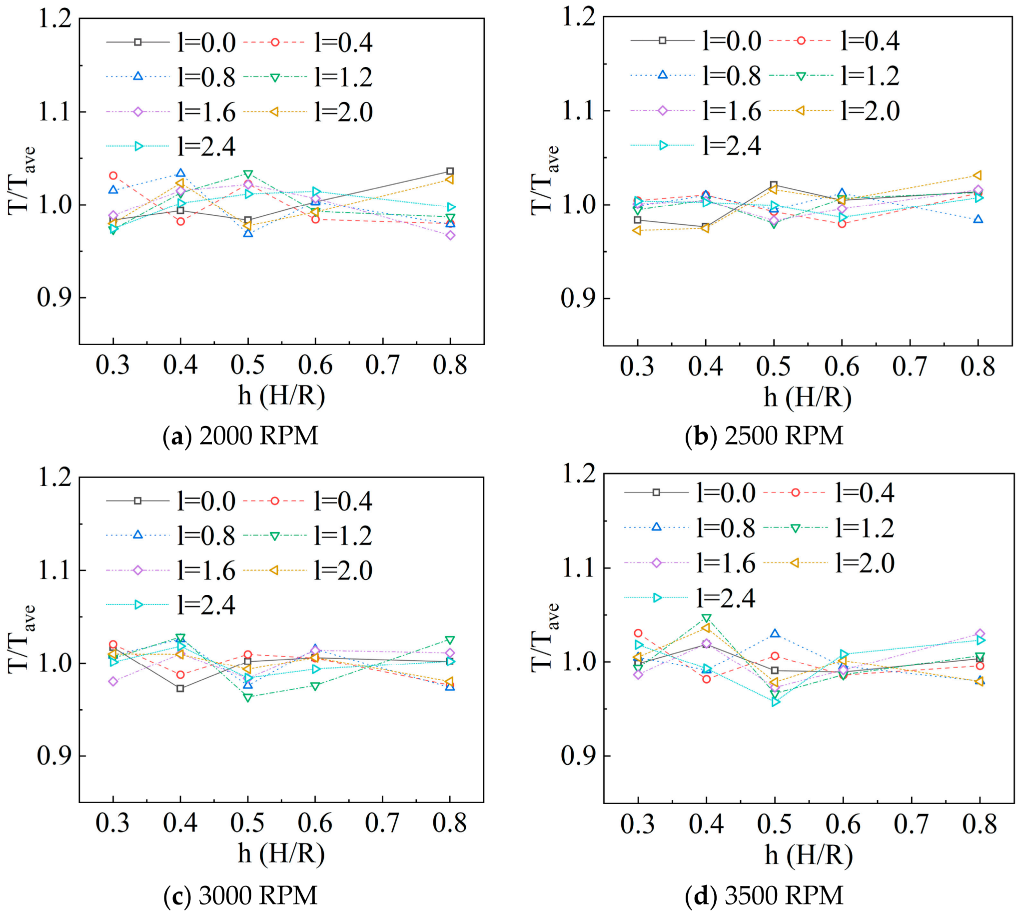

(**a**) 2000 RPM (**b**) 2500 RPM (**c**) 3000 RPM (**d**) 3500 RPM

Figure 16. The ratio of rotor thrust at different axial distances to the mean value.

Under different lateral conditions, the variation trends and amplitudes of rotor system thrust vary with changes in axial distance. Within the experimental axial distance range, at h = 0.8, there is a relatively large variation in thrust with lateral distance, with variation s reaching a maximum of 15% of the average value. On the other hand, at h = 0.3, the variation proportion is smaller, with variation s reaching a maximum of 12% of the average value.

Similarly, rotor system thrust exhibits significant variations with changes in lateral distance, as shown in Figure 17, fluctuating within the range of 85% to 115% of the average value under different axial distance conditions. This phenomenon is observed across various axial distance conditions. Interestingly, at a lateral distance of 0.4, rotor system thrust reaches its lowest values across different axial distance conditions, and in some cases even falls below that of the coaxial system. This phenomenon is most pronounced when the axial distance is at its highest value of 0.8. Furthermore, when comparing the thrust of the top and bottom rotors at different rotor speeds, taking 3000 RPM as an example, as shown in Figure 18, it becomes evident that the thrust of the top rotor generally decreases with increasing lateral distance, while the thrust of the bottom rotor rapidly increases after a lateral distance of 0.4. It stabilizes once the lateral distance reaches 2.0. Due to the faster rate of increase in thrust for the bottom rotor compared to the decrease in thrust for the top rotor, the overall rotor system thrust exhibits an upward trend, which aligns with the trend observed for the bottom rotor.

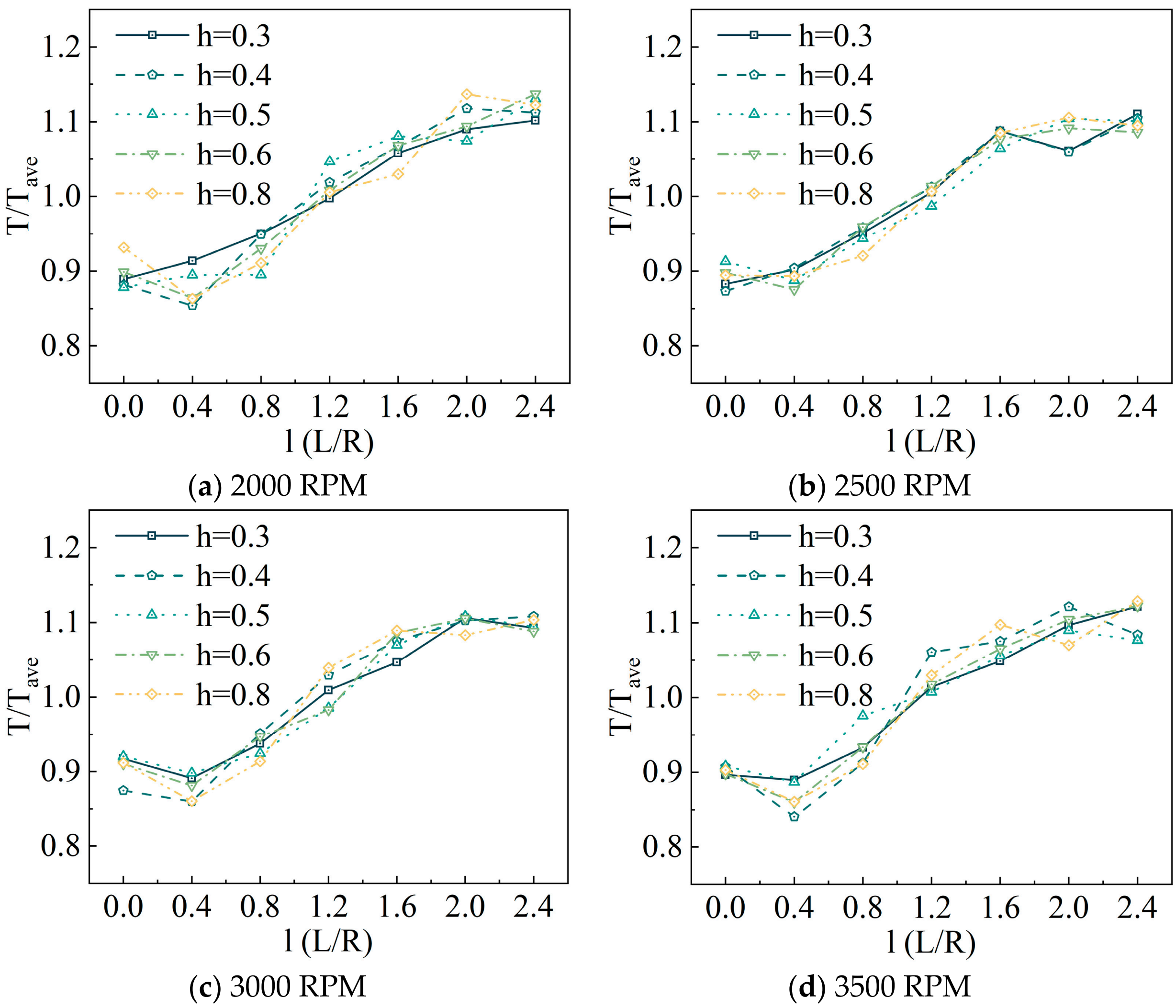

Figure 17. The ratio of rotor thrust at different lateral distances to the mean value.

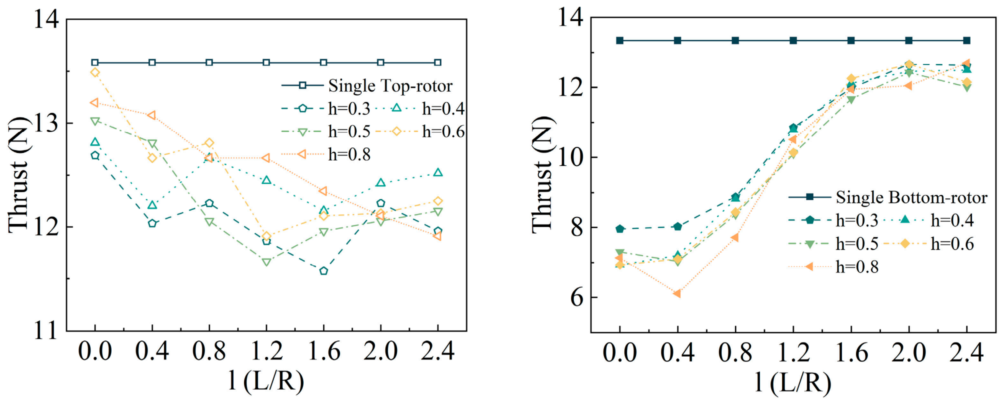

(**a**) Top rotor (**b**) Bottom rotor

Figure 18. The variation of rotor thrust with lateral distance at a rotor speed of 3000 RPM.

Figure 19 illustrates the trend of thrust variation with axial distance under constant rotor speed conditions at 3000 RPM. In the coaxial configuration, the thrust of the top rotor exceeds that of the top rotor under other lateral distances. However, in this configuration, the bottom rotor experiences greater thrust loss, resulting in lower system thrust. Nevertheless, it remains higher than the system thrust at a lateral distance of 0.4. When the lateral distance surpasses 1.6, the total system thrust levels become similar, influenced by the periodic rotor–vortex interference. The location of maximum thrust varies with different height spacings. To achieve maximum rotor system thrust performance, it is advisable to choose the optimal lateral spacing and layout based on the rotor's radius and axial distance when the lateral spacing is between 1.6 and 2.4. Across the entire range of lateral distances, the thrust for both top and bottom rotors is lower than that of a single rotor, but the system thrust is greater than that of a single rotor and less than twice the thrust of a single rotor.

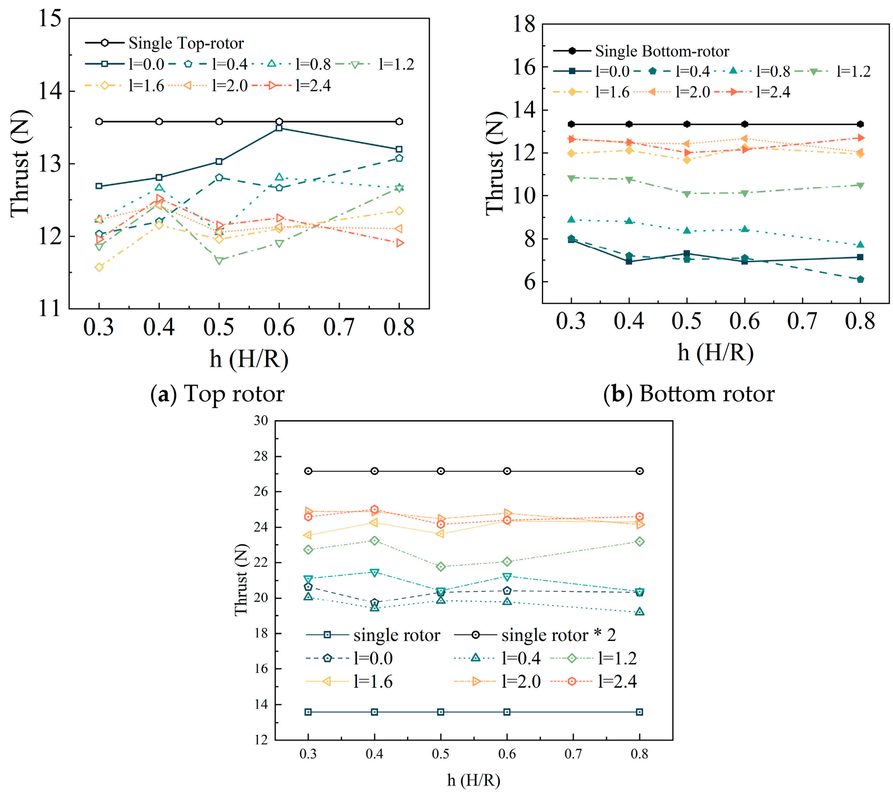

(**a**) Top rotor (**b**) Bottom rotor

(**c**) Total thrust

Figure 19. The variation of rotor thrust with axial distance at a rotor speed of 3000 RPM.

Figure 20 illustrates the variation of rotor thrust with axial and lateral distances at a rotor speed of 2000 RPM. Due to the correlation between the strength of blade tip vortices and rotor size and speed, the mutual interference effects differ when the relative positions of the two rotors are the same. Consequently, aiming solely for maximum thrust makes the search for the optimum positioning of the two rotors with respect to each other challenging. However, with the aid of fitted three-dimensional diagrams, a more intuitive observation reveals that, at the same horizontal spacing, rotor thrust exhibits minimal variation with vertical distance and significant variation with lateral distance. Based on the experimentally measured results, this information can guide the design of a more optimal rotor configuration.

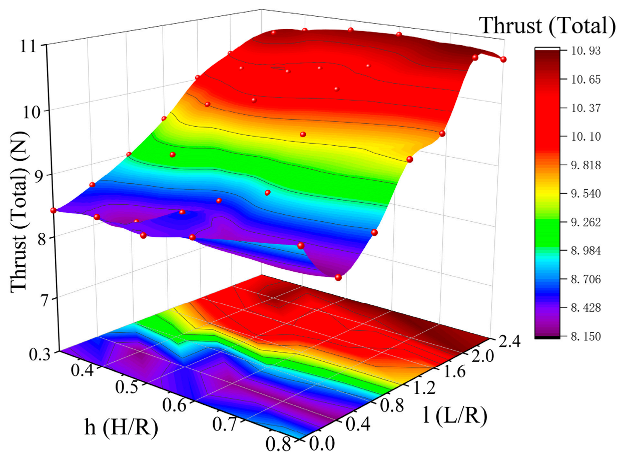

Figure 20. The variation of rotor thrust with axial distance and lateral distance at 2000 RPM.

4.4. Discussion

In previous studies, free-wake models [42] have been developed for tandem, tilt-rotor and coaxial rotor configurations. Despite the limitations in accuracy, these wake models could help understand the thrust variations presented in the paper. Thus, further discussion and validation could be carried out:

(1) During hover, although the wakes of both coaxial rotors contract, the wake contraction is more significant for the upper rotor due to the induced effect from the lower rotor. The tip vortices of the upper rotor, after passing through the lower rotor disc, consistently remain within the boundary of the lower rotor wake. Additionally, compared to the lower rotor, the wake of the upper rotor descends more rapidly. Thus, in the coaxial configuration, the thrust generated by the upper rotor is always greater than that of the lower rotor. Moreover, with an increase in axial distance, the measured thrust for the top and bottom rotors exhibits opposite trends. The thrust of the top rotor increases with axial distance, while the thrust of the bottom rotor decreases.

(2) In comparison to a single rotor, for coaxial dual rotors during hover, the induced velocity beneath the rotor is numerically larger for the same parameters. However, it is not a simple superposition of the induced velocities of two single rotors; instead, it is less than twice that of a single rotor. Similarly, the lift of coaxial dual rotors is greater than that of a single rotor but less than twice the lift of a single rotor.

(3) For the tandem configuration, a strong mutual interaction was observed between the tip vortices, resulting in a significant intermingling of tip vortices from the two rotors. Therefore, at a lateral distance of 0.4, the thrust of the rotor system reaches its lowest values across different axial distance conditions.

(4) Influenced by the downwash from the upper rotor, the induced velocity significantly increases in the region where the projections of the upper and lower rotors overlap. This is the main cause of lift loss for the lower rotor. When the stagger distance approaches 2.0, the boundary of the wake of the upper rotor coincides with the tip

region of the lower rotor, causing the disappearance of the tip vortices of the lower rotor. The upper rotor then produces an increased lifting effect on the tip of the lower rotor, leading to an increase in rotor lift. This phenomenon is consistent with the aerodynamic interference observed in the literature [43].

5. Conclusions

In this research, a small-scale rigid rotor aerodynamic force testbed was constructed. The constructed small-scale rigid rotor aerodynamic force testbed proved to be reliable and accurate for conducting experiments, with precise calculations and verification of experimental errors. Measurements of thrust for both top and bottom rotors were carried out across a range of parameters, including different axial distances, lateral distances and rotor speeds. The analysis revealed that the coaxial rotor system exhibited distinct aerodynamic interference patterns and aerodynamic force evolution trends under various parameter combinations. The key findings and conclusions are as follows:

1. Across various lateral or axial distance configurations, the variation in thrust with rotor speed follows an approximate quadratic trend and remains consistent with the thrust equation. For the top rotor, its thrust remains relatively stable in terms of magnitude and trend across different lateral or axial distance configurations, with minor differences at high speeds and variation s within 4% of the mean thrust. In contrast, the bottom rotor exhibits an increased rate of thrust growth with higher lateral distance, and the trend remains relatively consistent when the lateral distance exceeds 1.6.
2. Due to the vortex–vortex interaction, as the axial distance increases, the contribution of the top rotor to the total thrust increases, while the measured thrust for the top and bottom rotors shows opposite trends. Consequently, the overall system's total thrust remains relatively stable as the axial distance between the rotors increases.
3. Within the tested axial distance range, the variation trend of rotor system thrust with axial distance varies. At h = 0.8, there is significant thrust variation, with variation s reaching up to 15% of the mean thrust. At h = 0.3, the variation proportion is smaller, with variation s reaching up to 12% of the mean thrust.
4. The impact of axial distance on rotor system thrust is relatively small compared to the significant influence of lateral distance. Rotor system thrust exhibits substantial variation with changes in lateral distance, with values reaching as high as 115% of the mean thrust.
5. With increasing lateral distance, the impact of the top rotor's wake on the bottom rotor gradually diminishes, leading to a reduction in the difference between the thrust of the top and bottom rotors.
6. Due to mutual induction effects caused by rotor blade tip vortices, the thrusts of both rotors approach each other at a lateral distance of 1.6. At 2.0, the thrust of the bottom rotor surpasses that of the top rotor, and at 2.4, they approach each other again.
7. At a lateral distance of 0.4, the rotor system thrust for different axial distances reaches its lowest values.
8. Under various axial distance conditions, the variation trends in rotor system thrust with changes in lateral distance are similar. Within the tested lateral distance range, the largest variation proportion occurs at l = 1.2, while the smallest variation proportion occurs at l = 2.4.
9. Across different axial distance ranges, the thrust coefficients for both top and bottom rotors are lower than when a single rotor operates independently. Within different lateral distance ranges, the thrust for both top and bottom rotors is lower than that of a single rotor, but the system thrust exceeds that of a single rotor and is less than twice the thrust of a single rotor.

These conclusions provide valuable insights into the behavior and performance of staggered rotor systems, particularly concerning the impact of different parameters on aerodynamic interference and force evolution. In summary, the aerodynamic interference between rotors in a complex low Reynolds number operating environment results in diverse characteristics of thrust for top and bottom rotors under different lateral distances, axial distances and rotor speeds. This study has conducted relevant research and analysis to understand the impact of various parameters on rotor thrust. The findings highlight that rotor speed and lateral distance significantly influence the thrust performance of coaxial rotor systems, while axial distance also plays a role. Therefore, optimization of rotor system design considering these factors is essential. These results hold valuable insights for selecting appropriate relative positioning parameters of rotor systems to achieve optimal performance and efficiency.

In our forthcoming research endeavors, our objective is to incorporate power considerations, inflow angles and a broader range of rotor parameters into our investigations. This will necessitate ongoing refinement and optimization of our testbed to comprehensively assess the performance of rotor systems under various configurations.

Author Contributions: Conceptualization and methodology, H.Z.; validation, S.D. and S.W.; formal analysis, S.D. and S.W.; investigation, H.N. and X.W.; resources, H.N. and X.W. All authors have read and agreed to the published version of the manuscript.

Funding: This research was funded by the National Natural Science Foundation of China (H.Z., No. 52202443), China Postdoctoral Science Foundation (H.Z., 2023M731656), Natural Science Foundation of Jiangsu Province (H.Z., No. BK20220898) and Jiangsu Funding Program for Excellent Postdoctoral Talent (H.Z., No. JB0202003).

Data Availability Statement: The data presented in this study are available on request from the first author.

Conflicts of Interest: The authors declare no conflict of interest.

References

1. Thipphavong, D.P.; Apaza, R.D.; Barmore, B.E.; Battiste, V.; Belcastro, C.M.; Burian, B.K.; Dao, Q.V.; Feary, M.; Go, S.; Goodrich, K.H.; et al. Urban Air Mobility Airspace Integration Concepts and Considerations. In Proceedings of the 2018 Aviation Technology, Integration, and Operations Conference, Atlanta, GA, USA, 25–29 June 2018.
2. Zhang, H.; Zou, Y.; Zhang, Q.; Liu, H. Future urban air mobility management: Review. *Acta Aeronaut. Astronaut. Sin.* **2021**, *42*, 82–106.
3. Warwick, G. New Zealand Welcomes Flight Tests of Kitty Hawk's eVTOL Air Taxi. *Aviat. Week Space Technol.* **2018**, *180*, 28.
4. Rajendran, S.; Srinivas, S. Air taxi service for urban mobility: A critical review of recent developments, future challenges, and opportunities. *Transp. Res. Part E Logist. Transp. Rev.* **2020**, *143*, 102090.
5. Higgins, R.J.; Barakos, G.N.; Shahpar, S.; Tristanto, I. A computational fluid dynamic acoustic investigation of a tiltwing eVTOL concept aircraft. *Aerosp. Sci. Technol.* **2021**, *111*, 106571.
6. Holden, J.; Goel, N. Fast-Forwarding to a Future of On-Demand Urban Air Transportation. San Francisco, CA, 2016. Available online: https://evtol.news/__media/PDFs/UberElevateWhitePaperOct2016.pdf (accessed on 5 November 2023).
7. Miesner, S.; Schäferlein, U.; Keßler, M.; Krämer, E. High-fidelity Simulation of the Volocopter-2X in Cruise Flight. In Proceedings of the Vertical Flight Society 77th Annual Forum, Virtual, 10–14 May 2021.
8. Kim, H.D.; Perry, A.T.; Ansell, P.J. A Review of Distributed Electric Propulsion Concepts for Air Vehicle Technology. In Proceedings of the 2018 AIAA/IEEE Electric Aircraft Technologies Symposium (EATS), Cincinnati, OH, USA, 12–14 July 2018; pp. 1–21.
9. Palaia, G.; Abu Salem, K.; Cipolla, V.; Binante, V.; Zanetti, D. A Conceptual Design Methodology for e-VTOL Aircraft for Urban Air Mobility. *Appl. Sci.* **2021**, *11*, 10815.
10. Nugroho, G.; Hutagaol, Y.D.; Zuliardiansyah, G. Aerodynamic Performance Analysis of VTOL Arm Configurations of a VTOL Plane UAV Using a Computational Fluid Dynamics Simulation. *Drones* **2022**, *6*, 392.
11. Chahba, S.; Sehab, R.; Morel, C.; Krebs, G.; Akrad, A. Fast Sizing Methodology and Assessment of Energy Storage Configuration on the Flight Time of a Multirotor Aerial Vehicle. *Aerospace* **2023**, *10*, 425.
12. Ko, J.; Lee, S. Quantification of wake interaction effects on multi-rotor configurations in forward flight. *Aerosp. Sci. Technol.* **2023**, *135*, 108188. [CrossRef]
13. Lakshminarayan, V.K.; Baeder, J.D. High-Resolution Computational Investigation of Trimmed Coaxial Rotor Aerodynamics in Hover. *J. Am. Helicopter Soc.* **2009**, *54*, 42008.
14. Yoon, S.; Lee, H.C.; Pulliam, T.H. Computational Study of Flow Interactions in Coaxial Rotors. In Proceedings of the AHS Technical Meeting on Aeromechanics Design for Vertical Lift, San Francisco, CA, USA, 20–22 January 2016.
15. Passe, B.J.; Sridharan, A.; Baeder, J.D. Computational Investigation of Coaxial Rotor Interactional Aerodynamics in Steady Forward Flight. In Proceedings of the 33rd AIAA Applied Aerodynamics Conference, Dallas, TX, USA, 22–26 June 2015.

16. Yuan, M.; Liu, P.A.; Fan, F.; Jiang, L.; Lin, Y. Wind Tunnel Test Investigation of Coaxial Rigid Rotor Aerodynamic Interaction. *J. Nanjing Univ. Aeronaut. Astronaut.* **2019**, *51*, 257–262. [CrossRef]
17. Panjwani, B.; Quinsard, C.; Przemysław, D.G.; Furseth, J. Virtual Modelling and Testing of the Single and Contra-Rotating Co-Axial Propeller. *Drones* **2020**, *4*, 42. [CrossRef]
18. Hayami, K.; Sugawara, H.; Yumino, T.; Tanabe, Y.; Kameda, M. CFD analysis on the performance of a coaxial rotor with lift offset at high advance ratios. *Aerosp. Sci. Technol.* **2023**, *135*, 108194.
19. Benedict, M.; Winslow, J.; Hasnain, Z.; Chopra, I. Experimental Investigation of Micro Air Vehicle Scale Helicopter Rotor in Hover. *Int. J. Micro Air Veh.* **2015**, *7*, 231–255. [CrossRef]
20. Zhang, W.; Xu, B.; Zhang, H.; Xiang, C.; Fan, W.; Zhao, Z. Analysis of Aerodynamic Characteristics of Propeller Systems Based on Martian Atmospheric Environment. *Drones* **2023**, *7*, 397.
21. Zhang, T.; Barakos, G.N.; Furqan; Foster, M. High-fidelity aerodynamic and acoustic design and analysis of a heavy-lift eVTOL. *Aerosp. Sci. Technol.* **2023**, *137*, 108307.
22. Caprace, D.-G.; Ning, A.; Chatelain, P.; Winckelmans, G. Effects of rotor-airframe interaction on the aeromechanics and wake of a quadcopter in forward flight. *Aerosp. Sci. Technol.* **2022**, *130*, 107899. [CrossRef]
23. Tugnoli, M.; Montagnani, D.; Syal, M.; Droandi, G.; Zanotti, A. Mid-fidelity approach to aerodynamic simulations of unconventional VTOL aircraft configurations. *Aerosp. Sci. Technol.* **2021**, *115*, 106804.
24. Zanotti, A.; Savino, A.; Palazzi, M.; Tugnoli, M.; Muscarello, V. Assessment of a Mid-Fidelity Numerical Approach for the Investigation of Tiltrotor Aerodynamics. *Appl. Sci.* **2021**, *11*, 3385. [CrossRef]
25. Spyropoulos, N.; Papadakis, G.; Prospathopoulos, J.M.; Riziotis, V.A. Investigating the Level of Fidelity of an Actuator Line Model in Predicting Loads and Deflections of Rotating Blades under Uniform Free-Stream Flow. *Appl. Sci.* **2021**, *11*, 12097.
26. Thai, A.D.; De Paola, E.; Di Marco, A.; Stoica, L.G.; Camussi, R.; Tron, R.; Grace, S.M. Experimental and Computational Aeroacoustic Investigation of Small Rotor Interactions in Hover. *Appl. Sci.* **2021**, *11*, 10016.
27. Bohorquez, F. *Rotor Hover Performance and System Design of an Efficient Coaxial Rotary Wing Micro Air Vehicle*; ProQuest Information and Learning Company: Ann Arbor, MI, USA, 2007.
28. Ramasamy, M. Hover Performance Measurements Toward Understanding Aerodynamic Interference in Coaxial, Tandem, and Tilt Rotors. *J. Am. Helicopter Soc.* **2015**, *60*, 1–17. [CrossRef]
29. Zanotti, A.; Algarotti, D. Aerodynamic interaction between tandem overlapping propellers in eVTOL airplane mode flight condition. *Aerosp. Sci. Technol.* **2022**, *124*, 107518. [CrossRef]
30. Zhu, H.; Nie, H.; Zhang, L.M.; Wei, X.H.; Zhang, M. Design and assessment of octocopter drones with improved aerodynamic efficiency and performance. *Aerosp. Sci. Technol.* **2020**, *106*, 106206. [CrossRef]
31. Zhu, H.; Nie, H.; Zhang, L.M.; Deng, S.Q.; Wei, X.H. Aerodynamic Design Optimization of a Staggered Rotors Octocopter Based on Surrogate Model. *J. Aerosp. Eng.* **2021**, *34*, 481–500. [CrossRef]
32. Zhu, H.; Li, D.D.; Nie, H.; Wei, X.H.; Wei, Y.Z. Multiobjective optimization of a staggered-rotor octocopter design based on a surrogate model. *Aerosp. Sci. Technol.* **2023**, *139*, 108387. [CrossRef]
33. Zhu, H. Design and experimental testing of safe flight control system for novel vertical take-off and landing aircraft. *J. Vibroengineering* **2022**, *24*, 20. [CrossRef]
34. Otsuka, H.; Nagatani, K. Thrust loss saving design of overlapping rotor arrangement on small multirotor unmanned aerial vehicles. In Proceedings of the 2016 IEEE International Conference on Robotics and Automation (ICRA), Stockholm, Sweden, 16–21 May 2016.
35. Buzzatto, J.; Liarokapis, M. A Benchmarking Platform and a Control Allocation Method for Improving the Efficiency of Coaxial Rotor Systems. *IEEE Robot. Autom. Lett.* **2022**, *7*, 5302–5309. [CrossRef]
36. Weishupl, A.B.; Prior, S.D. Influence of Propeller Overlap on Large-Scale Tandem UAV Performance. *Unmanned Syst.* **2019**, *7*, 245–260. [CrossRef]
37. Brazinskas, M.; Prior, S.D.; Scanlan, J.P. An Empirical Study of Overlapping Rotor Interference for a Small Unmanned Aircraft Propulsion System. *Aerospace* **2016**, *3*, 32. [CrossRef]
38. Leishman, J.G.; Ananthan, S. An Optimum Coaxial Rotor System for Axial Flight. *J. Am. Helicopter Soc.* **2008**, *53*, 366–381. [CrossRef]
39. Kline, S.J.; Mcclintock, F.A. Describing Uncertainties in Single-Sample Experiments. *Mech. Eng.* **1953**, *75*, 2–8.
40. Leishman, J.G. *Principles of Helicopter Aerodynamics*; Cambridge University Press: New York, NY, USA, 2000.
41. Lakshminarayan, V.K.; Baeder, J.D. Computational Investigation of Microscale Coaxial-Rotor Aerodynamics in Hover. *J. Aircr.* **2010**, *47*, 940–955. [CrossRef]
42. Bagai, A.; Leishman, J.G. Free-Wake Analysis of Tandem, Tilt-Rotor and Coaxial Rotor Configurations. *J. Am. Helicopter Soc.* **1996**, *41*, 196–207. [CrossRef]
43. Guo Caigen, G.S. *General Design of Helicopter*; Aviation Industry Press: Beijing, China, 1993.